# Improved Accuracy of Cardiac Tissue-Level Simulations by Considering Membrane Resistance as a Cellular-Level Optimization Objective

E. Pouranbarani, *Student Member*, *IEEE*, L. A. Berg, R. S. Oliveira, R. W. dos Santos, and A. Nygren, *Member*, *IEEE*

***Abstract*— Cardiac cellular models are utilized as the building blocks for tissue simulation. One of the imprecisions of conventional cellular modeling, especially when the models are used in tissue-level modeling, stems from the mere consideration of cellular properties (e.g., action potential shape) in parameter tuning of the model. In our previous work, we put forward an accurate framework in which membrane resistance ($R_m$) reflecting inter-cellular characteristics, i.e., electrotonic effects, was considered alongside cellular features in cellular model fitting. This paper, for the first time, examines the hypothesis that considering $R_m$ as an additional optimization objective improves the accuracy of tissue-level modeling. To study this hypothesis, after cellular-level optimization of a well-known model, source-sink mismatch configurations in a 2-dimensional model are investigated. The results demonstrate that including $R_m$ in the optimization protocol yields a substantial improvement in the relative error of the critical transition border which is defined as the minimum window size between source and sink that wave propagates. Model developers can utilize the proposed concept during parameter tuning to increase the accuracy of models.**

***Index Terms*—Cardiac cellular models, tissue-level modeling, membrane resistance, inter-cellular characteristics, optimization.**

## I. Introduction

MATHEMATICAL models of cardiac cellular electrophysiology have been evolutionarily developed over the last 50 years [1]. Cellular computational models have broad applicability to the investigation of cardiac cellular functions and drug discovery fields as decision support tools [2], etc. Despite many improvements of *in silico* models, systematic methods for tuning the model parameters are still in their infancy [1].

Recently, studies have been conducted to present an optimization framework with the overall aims of eliminating the trial and error approach and considering cellular features as the target(s) of optimization [3-5]. The tuned models successfully reproduce cellular electrophysiological behavior; however, many of them fail in reproducing the properties that determine inter-cellular electrical interactions accurately. To address this problem, in our previous study [6], which was built on the work done by Kaur et al. [7], we proposed a robust optimization approach for cellular models that specifically accounts for inter-cellular behavior. In the following paragraphs, the principle of inter-cellular behaviors and electrotonic effects are described.

Electrical action potential ($AP$) propagation involves depolarizing the cells that receive charges (sink) from neighboring cells (source). If source charges are insufficient, conduction fails, which is known as source-sink mismatch. One circumstance in which source-sink mismatch may occur is the transition from a small volume of source to a large volume of sink. In this case, the electrotonic interaction between source and sink is functionally decreased, which may cause a block of the waveform in the transition border. However, in the inverse direction, the waveform can propagate successfully, resulting in a unidirectional block. This can be a potential mechanism for the onset of reentry in the unhealthy heart [8-11]. The Purkinje (source)-ventricular (sink) junction [12, 13], and connection parts of the sinoatrial node to atrial tissue [14] are examples where large electrotonic load can result in source-sink mismatch, failure of conduction, and arrhythmogenesis.

The importance of electrotonic effects in tissue modeling is emphasized in several studies [15, 16]. As the cellular models are the building blocks in the tissue models, capturing the properties of single cells that determine the electrotonic effect is essential during cell model development. Otherwise, misestimation of the $AP$ properties and diseases in the larger scale modeling may occur.

Membrane resistance ($R_m$) is a cellular characteristic that reflects the inter-cellular interaction (electrotonic effects) [17]. Although $R_m$ was taken into consideration in cellular model tuning in our previous work [6], to the best of our knowledge, the performance of the proposed framework at the tissue level has not been properly examined so far. Following from our previous work, in this paper, the parameters of the cellular model are first tuned. Subsequently, configurations based on tissue simulation (source-sink mismatch model) are defined to evaluate the effectiveness of utilizing $R_m$ as an additional criterion in the optimization.

## II. Materials and Methods

### A. Simulations of Cardiac Myocytes

The Ten Tusscher et al. (TNNP) model of human ventricle myocytes [18] is widely utilized in the study of cardiovascular characteristics. Here, to carry out simulations, we use TNNP as a model of study. The ionic current ($I_{ion}$) of this model

E. Pouranbarani and A. Nygren are with the Department of Electrical and Computer Engineering, University of Calgary, Alberta, Canada T2N 1N4 (e-mail: elnaz.pouranbarani@ucalgary.ca; nygren@ucalgary.ca).

L. A. Berg and R. W. dos Santos are with the Department of Computer Science and the Graduate Program of Computational Modeling, Federal University of Juiz de Fora, Juiz de Fora, Brazil (e-mail: berg@ice.ufjf.br; rodrigo.weber@ufjf.edu.br).

R. S. Oliveira is with the Department of Computer Science, University of São João del-Rei, São João del-Rei, Brazil (e-mail: sachetto@ufsj.edu.br).

which depends on the transmembrane voltage ($V_m$) and time ($t$), is obtained as follows:

$$C_m \frac{\partial V_m}{\partial t} = -I_{ion} + I_{stim}$$
$$I_{ion} = I_{Na} + I_{bNa} + I_{CaL} + I_{bCa} + I_{to} + I_{Kr} + I_{Ks} + I_{K1} + I_{pK} + I_{NaK} + I_{NaCa} + I_{pCa} \quad (1)$$

where $I_{stim}$ is stimulus current ($pA/pF$), and $C_m$ is the capacitance of the membrane ($\mu F/cm^2$).

### B. Calculation of Membrane Resistance

The procedure to calculate the $R_m$ in different phases of the $AP$ and justification for the selection of specific regions of $R_m$ profile are described in detail in [6]. Briefly, to obtain the $R_m$ in a specific voltage ($V_m$) value, $V_m$ is clamped to 10 $mV$ higher and lower of the original value in the separate simulations, and the corresponding currents are recorded after 5 $ms$ (inset in Fig. 1). The ratio of changes in voltage to the changes in current as a result of clamps gives the $R_m$ in that $V_m$ point. After obtaining the $R_m$ profile, the profile is divided into allowed and disallowed regions to avoid the selection of some singular points (pentagram in Fig. 1). For consideration of $R_m$ in parameter tuning, only $R_m$ values from allowed regions are selected.

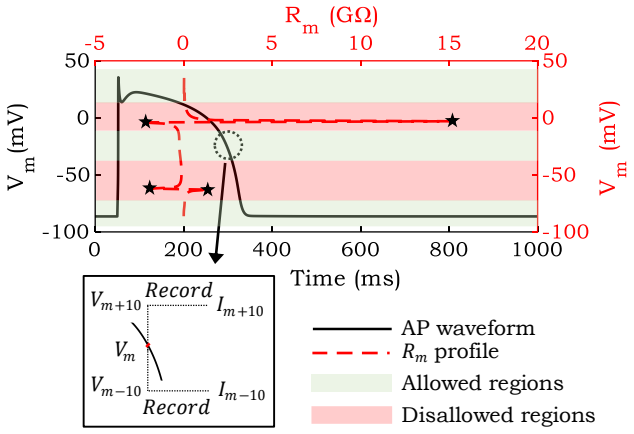


Fig. 1. Representation of $AP$ waveform, $R_m$ profile, and $R_m$ calculation.

### C. Optimization at the Cellular Level

The TNNP model with undetermined parameters is fitted to the original TNNP model (model-to-itself fitting). Fitness of $AP$, $(dv/dt)_{max}$ (maximum upstroke velocity), and $R_c$ (membrane resistance curve obtained from a part of the repolarization phase) are considered as three important cellular and intercellular objectives. These objectives are utilized with different combinations in various scenarios (Section III-A). Information about selected parameters and their boundaries can be found in [6].

Considering the relationship between $(dv/dt)_{max}$ and conduction velocity ($CV$) [19], in this paper, a modified version of our previous work [6] is employed to define the problem of optimization such that error of $(dv/dt)_{max}$ is considered as an additional cellular objective. This ensures that any difference in $CV$ of defined scenarios comparing to the reference scenario (Section III-A) in tissue does not result from inaccurate modeling the $(dv/dt)_{max}$, while the incorrect modeling of the $R_m$ gives rise to this inaccuracy.

After completing the optimization step, the resultant tuned parameters are used for tissue-level simulation (Section II-D).

### D. Tissue Simulation

The mathematical model of electrical propagation of $AP$ waveform is defined by a reaction-diffusion equation (the monodomain model). It is calculated as follows:

$$\beta \left(C_m \frac{\partial V_m}{\partial t} + I_{ion}(V_m, \eta)\right) + I_{stim} = \nabla \cdot (\sigma \nabla V_m) \quad (2)$$

$$\frac{\partial_\eta}{\partial_t} = f(V_m, \eta) \quad (3)$$

where $\beta$ is the surface per volume ratio ($cm^{-1}$), $\sigma$ is conductivity ($mS/cm$), and $\eta$ is the set of state variables.

The reaction and diffusion parts of Eq. 2 are divided by a splitting operator called Godunov [20] into a couple of distinct problems, i.e., a non-linear system of ordinary differential equations ($ODE$s) (Eq. 4) and parabolic partial differential equations ($PDE$s) (Eq. 5) that need to be solved in each time step.

$$\frac{\partial V_m}{\partial t} = \frac{1}{c_m}\left[-I_{ion}(V_m, \eta)) + I_{stim}\right] \quad (4)$$

$$\beta \left(C_m \frac{\partial V_m}{\partial t}\right) = \nabla \cdot (\sigma \nabla V_m) \quad (5)$$

Among various approaches, the Rush-Larsen and forward Euler methods are applied to solve Eq. 4 (related to cellular model), and the finite volume method (FVM) is utilized to solve the Eq. 5. A further description of this method is provided in [21]. In this study, tissue with the size of 10000 $\mu m \times$ 10000 $\mu m$ is simulated. The time step ($\Delta t$) is set to 0.01 $ms$ for solving both the reaction and diffusion equations, while the spatial discretization is set to 100 $\mu m$.

#### *Source-sink Mismatch Model*

Fig. 2 demonstrates the source-sink mismatch model used for the simulation. The size of connection part between source and sink is called the transition border ($W$); also, the critical transition border ($W_{critical}$) is defined as the smallest window size in which the wave propagates. Therefore, to calculate critical window size, we increase the $W$ from small values until a successful wave propagation occurs. A current with 50 $pA/pF$ amplitude and 2 $ms$ duration is injected to 1000 $\mu m \times$ $W$ rectangular region located at the source site. The length ($L$) of source and sink is the same, and equal to 5000 $\mu m$ (Fig. 2).

Two criteria need to be satisfied to reach a successful propagation: 1) Cells should reach their threshold voltage to produce an $AP$. 2) Charges of each cell must be enough to deliver to their adjacent cells. If a cell reaches the threshold with delay, excitation of neighboring cells will be happening at a later time, resulting in decreased $CV$. This phenomenon reduces the percentage of available source charges to required sink charges (safety factor) that yields source-sink mismatch

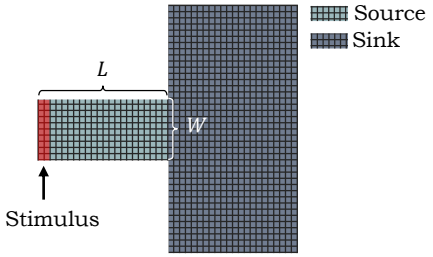


Fig. 2. A schematic illustration of the source-sink mismatch model.

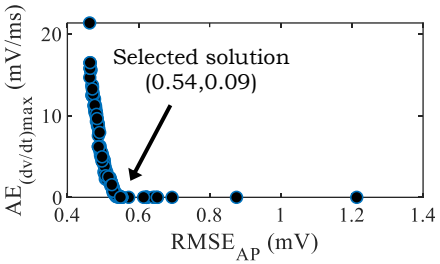


Fig. 3. An example of the Pareto front in *Scenario* 2.

[9]. To evaluate the efficacy of different scenarios which are defined in Section III-A, we decrease the $CV$ by reducing $\sigma$ of the source in all directions ($\sigma_x$, $\sigma_y$) with different source factors ($f_i$). Therefore, the impact of longitudinal and transversal electrotonic effects is determined. In other words, differences in electrotonic effects among scenarios in different conditions can be investigated.

## III. Results

### A. Case Studies

In this paper, three scenarios are considered for the simulations. In *Scenario* 1, the TNNP with original parameter values is utilized. In *Scenarios* 2 and 3, the model parameters are modified based on tuned parameters obtained from the optimization protocol. The parameters of *Scenario* 2 are calculated by considering fitness of $AP$ and $(dv/dt)_{max}$. For *Scenario* 3, the parameters are optimized by fitting the $AP$, $(dv/dt)_{max}$, and $R_c$. The conductivities of the sources are decreased by factors of 9 and 10 in the independent simulations.

Our previous formulation, which is defined in [6], is applied to select an optimal solution of *Scenario* 2. To visualize the trade-off among objectives, the Pareto front for one of the trials is depicted in Fig. 3. To ensure a fair comparison among the scenarios, in *Scenario* 3 a solution with errors of $AP$ and $(dv/dt)_{max}$ similar to *Scenario* 2 is chosen. The reason is that our main aim for comparison between scenarios is to show the effectiveness of considering $R_c$ in the optimization protocol on the tissue behavior. To evaluate the performance of *Scenarios* 2 and 3, two independent simulations are conducted. Also, due to the importance of $R_d$ (membrane resistance value in the rest phase), $R_d$ is calculated *a posteriori* for comparison. Table I demonstrates the average (Ave.), and standard deviations (Std.) of root mean square error ($RMSE$) of $AP$ ($RMSE_{AP}$) and $R_c$ ($RMSE_{R_c}$) as well as the absolute error ($AE$) of $(dv/dt)_{max}$ ( $AE_{(dv/dt)_{max}}$) and $R_d$ ($AE_{R_d}$) of two trials in *Scenarios* 2 and 3 with respect to *Scenario* 1.

TABLE I
AVERAGE AND STANDARD DEVIATIONS OF $RMSE_{AP}$, $AE_{(dv/dt)_{max}}$, $RMSE_{R_c}$, AND $AE_{R_d}$ OF TRIALS IN *SCENARIO* 2 (S2) AND *SCENARIO* 3 (S3).

| Scenarios | $RMSE_{AP}$ ($mV$) | | $AE_{(dv/dt)_{max}}$ $mV/ms$ | | $RMSE_{R_C}$ (MΩ) | | $AE_{R_d}$ (MΩ) | |
|---|---|---|---|---|---|---|---|---|
| | Ave. | Std. | Ave. | Std. | Ave. | Std. | Ave. | Std. |
| S2 | 0.43 | 0.15 | 0.06 | 0.05 | 34.54 | 9.66 | 1.62 | 0.53 |
| S3 | 0.41 | 0.11 | 0.06 | 0.03 | 4.26 | 0.18 | 0.47 | 0.02 |

### B. Source-sink Mismatch Model

In the source-sink mismatch model, if the width of the channel ($W$) is larger than a specific value, which depends on the source factor ($f$), the wave propagates. The comparisons of critical transition border between scenarios in two different $f$s are illustrated in Fig. 4. As can be seen from this figure, in *Scenario* 1, which is the target of our comparison with other scenarios, the propagations happen in $W_{critical} = 2800\ \mu m$ and 2200 $\mu m$ in $f_1$=1/10 and $f_2$=1/9, respectively. However, $W_{critical}$ corresponding to trials of *Scenario* 2 with different source factors (Fig. 4 (a)) are significantly different from *Scenario* 1. Fig. 4 (a) shows that $W_{critical}$ in *Scenario* 2 deviates up to 600 $\mu m$ (trial 1, $f_1$=1/10). The different behavior of *Scenario* 2 in various trials and source factors comparing to *Scenario* 1, confirms that consideration of only cellular properties is not sufficient to tune the model parameters. In this regards, *Scenario* 3 in which $R_c$ is included as an additional objective is defined. $W_{critical}$ in the trials of *Scenario* 3 is also represented in Fig. 4 (b). This figure clearly shows that including $R_c$ in the optimization results in improvement of tissue behavior (source-sink) in tissue-level modeling.

Another representation of differences between scenarios is provided for one of the trials (trial 1) in Fig. 5. Fig. 5 (a) and (b) show snapshots of the source-sink mismatch model in $f_1$=1/10 at t=137 $ms$ and 154 $ms$ for *Scenarios* 1-3, respectively. Although in all scenarios the waves propagate, the propagation velocity of *Scenario* 2 is considerably different. Therefore, the behavior of *Scenario* 3 is more

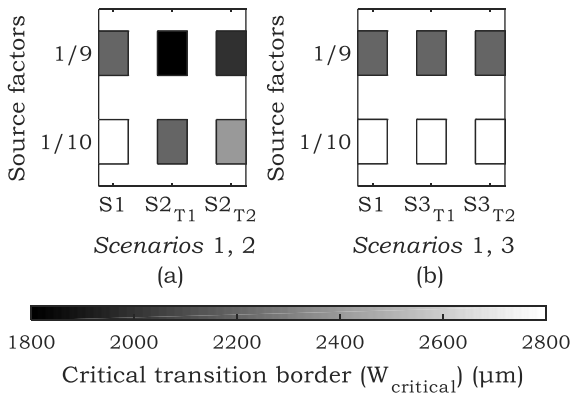


Fig. 4. Comparison of critical transition border ($\mu m$) in source factors=1/10 and 1/9, a) *Scenario* 1 (S1) and trials of *Scenario* 2 ($S2_{Ti}$, $i$=1, 2), b) S1 and trials of *Scenario* 3 ($S3_{Ti}$, $i$=1, 2).

similar to *Scenario* 1, and this verifies that *Scenario* 3 is more robust comparing to *Scenario* 2.

## IV. Discussion

Tissue-level simulations demonstrate that as a result of considering intercellular electrotonic effects during the cellular optimization process (*Scenario* 3), the accuracy of source-sink mismatch modeling is significantly improved. On the other hand, in *Scenario* 2, in which the electrotonic effects during the optimization process are disregarded, the critical transition border (factor of comparison among scenarios) is different compared to *Scenario* 1. While in this *Scenario*, $AP$ and $(dv/dt)_{max}$ matches *Scenario* 1 with high accuracy at the cellular level. In line with these preliminary results, additional investigations need to be conducted to further understand the impact of the $R_m$ on various aspects of tissue-level modeling.

## V. Conclusions

Consideration of membrane resistance as an indicator of intercellular property, during cellular parameter tuning, improves the tissue-level simulations. As proof of concept, this claim is evaluated for two different source factors of the source-sink mismatch model. The results confirm the efficacy of the proposed concept for accurately simulating the propagation in tissue-level modeling. This study paves the way for the precise development of cellular models, thereby enhancing the understanding of cardiac diseases.

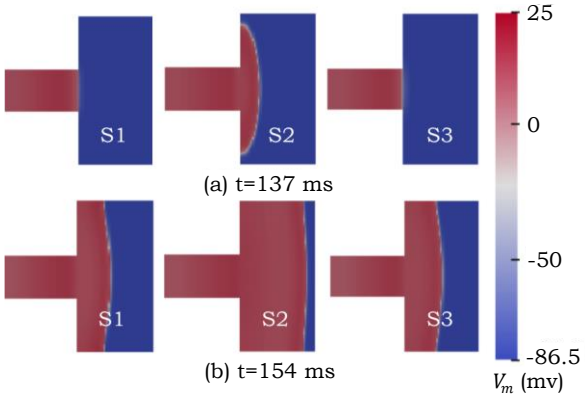


Fig. 5. An example of a snapshot of the source-sink mismatch model in $f_1$=1/10 for *Scenarios* 1-3 (S1-S3). a) Time=137 $ms$, b) Time=154 $ms$. The size of transition border is 2800 $\mu m$.

## References


[1] T. Krogh-Madsen, E. A. Sobie, and D. J. Christini, "Improving cardiomyocyte model fidelity and utility via dynamic electrophysiology protocols and optimization algorithms," *J. Physiol.,* vol. 594, no. 9, pp. 2525-2536, May 2016.

[2] M. R. Davies *et al.*, "Recent developments in using mechanistic cardiac modelling for drug safety evaluation," *Drug Discov. Today,* vol. 21, no. 6, pp. 924-938, June 2016.

[3] S. Dokos and N. H. Lovell, "Parameter estimation in cardiac ionic models," *Prog. Biophys. Mol. Biol.,* vol. 85, no. 2-3, pp. 407-431, 2004.

[4] Z. Syed, E. Vigmond, S. Nattel, and L. Leon, "Atrial cell action potential parameter fitting using genetic algorithms," *Med. Biol. Eng. Comput.,* vol. 43, no. 5, pp. 561-571, Oct 2005.

[5] E. Pouranbarani and A. Nygren, "A Novel Bi-Level Framework for Fitting the Parameters in Cardiac Cellular Models," *40th Annual International Conference of the IEEE Eng. in Medicine and Biology Society (EMBC)*, 2018, pp. 2370-2373.

[6] E. Pouranbarani, R. W. dos Santos, and A. Nygren, "A robust multi-objective optimization framework to capture both cellular and intercellular properties in cardiac cellular model tuning: Analyzing different regions of membrane resistance profile in parameter fitting," *PLoS One,* vol. 14, no. 11, Nov. 2019.

[7] J. Kaur, A. Nygren, and E. J. Vigmond, "Fitting membrane resistance along with action potential shape in cardiac myocytes improves convergence: application of a multi-objective parallel genetic algorithm," *PLoS One,* vol. 9, no. 9, p. e107984, 2014.

[8] A. G. Kléber and Y. Rudy, "Basic mechanisms of cardiac impulse propagation and associated arrhythmias," *Physiol. Rev.,* vol. 84, no. 2, pp. 431-488, 2004.

[9] P. Spector, "Principles of cardiac electric propagation and their implications for re-entrant arrhythmias," *Circ: Arrhythm. Electrophysiol.,* vol. 6, no. 3, pp. 655-661, 2013.

[10] S. Dhein *et al.*, "Remodeling of cardiac passive electrical properties and susceptibility to ventricular and atrial arrhythmias," *Front. Physiol.,* vol. 5, p. 424, 2014.

[11] E. J. Ciaccio, J. Coromilas, A. L. Wit, N. S. Peters, and H. Garan, "Source-sink mismatch causing functional conduction block in re-entrant ventricular tachycardia," *JACC: Clinical Electrophysiol.,* p. 519, 2017.

[12] D. J. Huelsing, K. W. Spitzer, J. M. Cordeiro, and A. E. Pollard, "Conduction between isolated rabbit Purkinje and ventricular myocytes coupled by a variable resistance," *Amer. Journal Physiol.,* vol. 274, no. 4, pp. H1163-H1173, 1998.

[13] O. V. Aslanidi, P. Stewart, M. R. Boyett, and H. Zhang, "Optimal velocity and safety of discontinuous conduction through the heterogeneous Purkinje-ventricular junction," *Biophys. J.,* vol. 97, no. 1, pp. 20-39, 2009.

[14] S. D. Unudurthi, R. M. Wolf, and T. J. Hund, "Role of sinoatrial node architecture in maintaining a balanced source-sink relationship and synchronous cardiac pacemaking," *Front. Physiol.,* vol. 5, p. 446, 2014.

[15] R. Weber dos Santos, A. Nygren, F. Otaviano Campos, H. Koch, and W. R. Giles, "Experimental and theoretical ventricular electrograms and their relation to electrophysiological gradients in the adult rat heart," *Amer .J. Physiol.,* vol. 297, no. 4, pp. H1521-H1534, 2009.

[16] C. M. Costa, P. A. A. Silva, and R. W. dos Santos, "Mind the gap: a semicontinuum model for discrete electrical propagation in cardiac tissue," *IEEE Trans. Biomed. Eng.,* vol. 63, no. 4, pp. 765-774, 2015.

[17] K. W. Spitzer, A. E. Pollard, L. Yang, M. Zaniboni, J. M. Cordeiro, and D. J. Huelsing, "Cell-to-cell electrical interactions during early and late repolarization," *J. Cardiovas. Electrophysiol.,* vol. 17, pp. S8-S14, 2006.

[18] K. Ten Tusscher, D. Noble, P.-J. Noble, and A. V. Panfilov, "A model for human ventricular tissue," *Amer. J. Physiol.,* vol. 286, no. 4, pp. H1573-H1589, 2004.

[19] J. W. Buchanan Jr, T. Saito, and L. S. Gettes, "The effects of antiarrhythmic drugs, stimulation frequency, and potassium-induced resting membrane potential changes on conduction velocity and dV/dtmax in guinea pig myocardium," *Circ. Res,* vol. 56, no. 5, pp. 696-703, 1985.

[20] J. Sundnes, G. T. Lines, X. Cai, B. F. Nielsen, K.-A. Mardal, and A. Tveito, *Computing the electrical activity in the heart*. Berlin Heidelberg: Springer-Verlag, 2006.

[21] R. Sachetto Oliveira, B. Martins Rocha, D. Burgarelli, W. Meira Jr, C. Constantinides, and R. Weber dos Santos, "Performance evaluation of GPU parallelization, space-time adaptive algorithms, and their combination for simulating cardiac electrophysiology," *Int. J. for Numer. Methods Biomed. Eng.,* vol. 34, no. 2, p. e2913, 2018.